Detection of demyelination in multiple sclerosis by analysis of T_2^* relaxation at 7 T

Xiaozhen Li [a,b,*], Peter van Gelderen [a], Pascal Sati [c], Jacco A. de Zwart [a], Daniel S. Reich [c], Jeff H. Duyn [a]

[a] Advanced MRI Section, Laboratory of Functional and Molecular Imaging, National Institute of Neurological Disorders and Stroke, National Institutes of Health, Bethesda, MD 20892, USA
[b] Department of Neurobiology, Care Sciences and Society, Division of Clinical Geriatrics, Center for Alzheimer Disease Research, Karolinska Institutet, Stockholm SE-141 57, Sweden
[c] Translational Neuroradiology Unit, Division of Neuroimmunology and Neurovirology, National Institute of Neurological Disorders and Stroke, National Institutes of Health, Bethesda, MD 20892, USA

ARTICLE INFO

ABSTRACT

Multiple sclerosis (MS) is a relatively common cause of inflammatory demyelinating lesions of the central nervous system. In an attempt to detect and characterize ongoing demyelination in MS patient brains, we used a novel magnetic resonance imaging (MRI) technique, involving the fitting of a three-component model to the T_2^* relaxation behavior at high-field (7 T). This model allowed estimation of the amount of myelin water (and thus indirectly myelin content), axonal water, and interstitial water. In this study, 25 relapsing–remitting MS patients underwent a 7 T MRI from which 12 gadolinium-enhancing lesions, 61 non-enhancing lesions, and their corresponding contralateral normal appearing white matter (NAWM) regions were analyzed. In both enhancing and non-enhancing lesions, the amplitude of myelin water was significantly decreased, and interstitial and axonal water were increased relative to the contralateral NAWM. Longer relaxation time T_2^* of interstitial and axonal water, and lower frequency shift of axonal water, were also observed in both enhancing and non-enhancing lesions when compared to the contralateral NAWM. No significant difference was found between enhancing lesions and non-enhancing lesions. These findings suggest that the fitting of a three-component model to the T_2^* decay curve in MS lesions may help to quantify myelin loss.

Published by Elsevier Inc. This is an open access article under the CC BY-NC-ND license
(http://creativecommons.org/licenses/by-nc-nd/4.0/).

1. Introduction

Multiple sclerosis (MS) is a chronic, inflammatory, demyelinating disease of the central nervous system characterized by the formation of focal demyelinated regions ('plaques' or 'lesions'). For the last quarter century, magnetic resonance imaging (MRI) has been routinely used to help with the diagnosis of MS, as well as to monitor disease evolution and treatment efficacy. However, the mechanisms underlying the clinical progression of MS and the relationship of MRI findings to pathology (demyelination, axonal loss and neuronal degeneration) remain poorly understood. Meanwhile, numerous studies have attempted to more specifically assess the demyelination process occurring in MS by measuring indirectly the local myelin content using various MR techniques, such as diffusion tensor imaging, magnetization transfer (MT) imaging, and separation of T_2 relaxation components (Laule et al., 2007). The separation of T_2 relaxation components has been used to measure the amount of water trapped between the myelin layers, which is generally considered to reflect brain myelin content. This is based on the fact that the diffusion-restricting properties of myelin lead to distinct T_2 values for water between the myelin layers (or myelin water), intra-axonal water, and interstitial water (or extracellular water), with the myelin water pool having the shortest T_2 (Lancaster et al., 2003; Laule et al., 2004; Andrews et al., 2005; MacKay et al., 2006). With this model in mind, these studies have tried to assess the relative concentration of myelin water using mathematical analyses of the T_2 relaxation decay curves acquired with a multi-spin-echo (mSE) technique. Strong correlation between the short T_2 signal fraction and the anatomical distribution of myelin was found in postmortem MS brain samples (Moore et al., 2000; Laule et al., 2006; Laule et al., 2008), supporting the notion that this fraction reflects myelin water. Absence of myelin water signal was also found in chronic demyelinated MS lesions (Moore et al., 2000). The post mortem findings were further supported by in vivo studies that also reported decreased amount of myelin water in MS lesions (MacKay et al., 1994; Vavasour et al., 1998; Laule et al., 2004).

More recently, multi-gradient-echo (mGRE) techniques have been proposed as another way to obtain cellular compartment-specific information (Du et al., 2007; Hwang et al., 2010; van Gelderen et al., 2012; Sati et al., 2013). Similar to the T_2-based method, the premise is that

the myelin-associated water has a distinctly decreased T_2^* and that the exchange between the free and myelin water pools is slow enough to observe non-mono-exponential T_2^* decay as a function of echo time (TE) for myelin-containing tissue (van Gelderen et al., 2012). Therefore, information about myelin water can also be gained from multi-component fitting of the T_2^* relaxation decay curve. Moreover, compared to mSE-based acquisition measurements, it has been reported that mGRE-based acquisition for mapping T_2^* provides higher contrast-to-noise ratio in structural MRI and BOLD fMRI (Duyn et al., 2007) and lower radiofrequency power deposition at high magnetic field strengths. Another advantage of the three-component T_2^* model is that it provides frequency information, which improves the discrimination between myelin, axonal, and interstitial water due to their different frequency shifts (van Gelderen et al., 2012; Sati et al., 2013). Therefore, in addition to demyelination, this model might provide new insights into axonal injury and degenerative processes.

The fitting of a three-component model to T_2^* decay curves acquired at 7 T was recently evaluated in healthy human brains (Sati et al., 2013), but the feasibility of this technique in MS patients, and what it uncovers about lesion biology, remains to be demonstrated. For this purpose, mGRE data were acquired in cohort of MS patients at 7 T to investigate whether the fitting of a three-component model to the T_2^* decay curve can be used for characterizing demyelination in patient brains.

2. Materials and methods

2.1. Subjects

Twenty-five relapsing–remitting MS (RRMS) patients (6 men, 19 women; age range, 30–63 years; mean 41 years; standard deviation 8.4) were recruited from August 2013 to May 2014 under an Internal Review Board approved human protocol. Experienced MS clinicians determined disability according to the Expanded Disability Status Scale (EDSS) and obtained clinical data. Median EDSS score was 1.5 (range = 1–6.5) and mean disease duration was 8.5 years (range = 0.3–21.6 years).

2.2. MRI acquisition

All MRI examinations were performed on a 7 T human MRI scanner (Siemens, Erlangen, Germany) equipped with a 32-channel receive coil.

The mGRE data for mapping the T_2^* decay curves were acquired with an in-house developed pulse-sequence (van Gelderen et al., 2012). Echo times (TEs) ranged from 2.3 to 62.7 ms. Thirty-eight echoes (positive read gradient only) were acquired with an echo spacing of 1.6 ms. Repetition time (TR) was 1 s and flip angle (FA) was 70°. Fifteen slices with 1.5 mm slice thickness and 25% gap between slices were measured per scan, with an in-plane resolution of 1.5 × 1.5 mm and a FOV of 240 × 180 mm (the acquisition matrix size is 160 × 120). The slices were parallel to the plane of the anterior and posterior commissure line and captured a section of the corpus callosum. Five signal averages were acquired within a total scan time of 10 min.

Whole brain 3D T_1-weighted magnetization-prepared rapid gradient echo (T_1-MPRAGE) was acquired before (pre-gad T_1) and after (post-gad T_1) contrast injection (0.1 mmol/kg gadobutrol; Bayer Healthcare, Leverkusen, Germany).

2.3. Imaging reconstruction and fitting of a three-component model to the T_2^* decay curves

All mGRE data analyses were performed in Interactive Data Language (IDL, Exelis Visual Information Solutions, Boulder, CO, USA).

The complex images were combined from individual receiver channels using unaccelerated (rate-1) SENSE reconstruction (Pruessmann et al., 1999), then co-registered based on the fourth echo of the first repetition, since increased image contrast at this TE is expected to increase

registration performance. The phase corrections before fitting consisted of two steps, one was a function of echo time, the other a spatial correction. Step one: in every voxel the average offset frequency was subtracted based on a linear fit (over TE) to the phase of the echoes, accounting for possible 2π wrapping jumps. Step two: for each echo time, a spatial linear phase was subtracted, that is for every image the global phase and the in-plane (spatial) gradients were taken out. The complex images were normalized to the smoothed magnitude image at first echo (TE = 2.3 ms). Smoothing was accomplished by Gaussian filtering over 30 voxels within a brain mask, excluding the skull and extracerebral cerebrospinal fluid, to preserve the contrast between lesions and their surrounding tissue. Normalization to a smoothed image was performed to remove both scan-to-scan variability and residual receive coil sensitivity effects, while preserving increased signal intensity in lesions due to their higher water content.

Using normalized T_2^*-weighted mGRE magnitude images (20th echo, TE = 33.6 ms), regions of interest (ROIs) were drawn manually in the splenium of the corpus callosum (SCC) (Fig. 1a) and the optic radiations (OR) (Fig. 1b), excluding visible lesions, to check the reproducibility of the fitting of the three-component model to the T_2^* decay curve. Furthermore, ROIs were chosen in all lesions visible on these T_2^*-weighted mGRE magnitude images (20th echo, TE = 33.6 ms) (Fig. 2a) for each scan. Lesions were identified by hyperintensity on these same normalized T_2^*-weighted mGRE magnitude images (20th echo, TE = 33.6 ms), because myelin decreases T_2^* and thus myelin loss leads to brighter intensity on the T_2^*-weighted image. In addition, control ROIs (Fig. 2b, blue) were chosen in normal appearing white matter (NAWM) with a size and shape similar to the lesions. Any visible veins, which were low image intensity on T_2^*-weighted mGRE, were excluded from all the ROIs. Enhancing lesions were identified from post-gad T_1-MPRAGE (Fig. 3c and f).

Similarly to our previous study (Sati et al., 2013), the ROI-averaged complex signal S was calculated and fitted with a three-component model using the following equation.

$$S = (A_1 e^{(-1/T_{2,1}^* + i2\pi\Delta f_1)t} + A_2 e^{(-1/T_{2,2}^* + i2\pi\Delta f_2)t} + A_3 e^{(-1/T_{2,3}^*)t})e^{i(2\pi f_g t + \varphi)}.$$

Here, A_n is the amplitude, $T_{2,n}^*$ is the relaxation time, and Δf_n is the frequency shift of component n, which is defined relative to global/interstitial water frequency f_g. φ is the phase offset. Components 1, 2 and 3 were assigned to myelin, axonal and interstitial water respectively (van Gelderen et al., 2012; Sati et al., 2013). Based on our preliminary data, the starting values for the fitting were defined as $A_1 = 0.16$, $A_2 = 0.43$, $A_3 = 0.41$; $T_{2,1}^* = 6.3 ms$, $T_{2,2}^* = 41.7 ms$, $T_{2,3}^* = 26.3 ms$; $\Delta f_1 = 21$ Hz, $\Delta f_2 = -6$ Hz, $f_g = 0$ Hz, and $\varphi = 0$ Hz. For the analyses of lesions, the $T_{2,1}^*$ and Δf_1 were fixed at values from contralateral NAWM as the myelin water signal in lesions proved to be too small to determine these independently. A range of values was tested, which did not change the results significantly (supplementary table).

2.3.4. Statistical analyses

Statistical analysis was carried out using a two-tailed Student's t-test to investigate differences between enhancing lesions and NAWM, non-enhancing lesions and NAWM, and enhancing versus non-enhancing lesions for the three-component fitting results. The significance threshold was taken as $p < 0.05$.

3. Results

Twelve enhancing lesions were detected in 7 patients, these appeared on both post-gad T_1-MPRAGE and magnitude images. Sixty-one non-enhancing lesions were included in the study. Voxel-level image average SNR was approximately 200:1 in the first echo in the ROIs examined. The average size of lesions was 77.6 mm³ (range 10.1–253.1 mm³) (Table 1). In total, 25 ROIs in SCC and OR, as well as

73 lesions and their corresponding contralateral NAWM ROIs, were analyzed using the fitting of a three-component model to the T_2^* decay curve.

As seen in Fig. 4 and Table 1, the model described the mGRE data. Goodness of fit was assessed using the $1\text{-}R^2$ values, where R^2 is the coefficient of determination (Colin Cameron and Windmeijer, 1997) and indicates how well the data fit the decay curve. A R^2 of 1 would indicate that the model perfectly fits the decay curve. All $1\text{-}R^2$ values were lower than 0.001, which means that over 99.99% of the variance was explained using this model. The residues were further evaluated by comparing temporal standard deviation to the thermal noise level in the ROI-averaged signal. Note that this noise level varies notably from one ROI to the next, since it depends on the number of voxels averaged and thus on ROI size.

Results from the fitting of this three-component model for the different ROIs (SCC, OR, lesion and contralateral NAWM) are shown in Table 2. The average amplitude of myelin water (A_1) was 0.12 in SCC and 0.10 in both OR and NAWM, but only approximately 0.03 in lesions. As expected, the T_2^* of myelin water was the shortest, whereas the axonal water had the longest T_2^*. Myelin water showed the largest frequency shift (25.8 Hz in SCC), whereas that of axonal water was small and negative (-6.3 Hz in SCC). The frequency shift of myelin water was smaller in NAWM than in SCC and OR, presumably due to orientation effects.

In both enhancing and non-enhancing lesions, the amplitude of myelin water (A_1) was found to be significantly decreased ($\Delta A_1 \sim 0.07$, $p < 0.001$) compared to contralateral NAWM. Since one would expect reductions in A_1 to be accompanied by increases in T_2^* and thus signal intensity (S) at longer echo times in the mGRE images, this relationship was investigated by generating a scatter plot (Fig. 5) in which the fitted myelin water amplitude (A_1) was plotted as a function of the signal intensity (S) in the normalized 20th echo (33.6 ms TE) mGRE magnitude image ($S_{TE = 33.6}$). Indeed, a significant correlation ($R = 0.61$, $p < 0.001$) and a negative slope (0.21) between the two parameters are seen, which appears dominated by the differences between lesions and NAWM.

The axonal water amplitude (A_2) was found to be increased in both enhancing lesions ($\Delta A_2 = 0.04$, $p < 0.05$) and non-enhancing lesions ($\Delta A_2 = 0.04$, $p < 0.001$) in comparison to NAWM. In the comparison of interstitial water amplitude (A_3) between lesions and NAWM, the interstitial water amplitude (A_3) in enhancing lesions increased 0.06 ($p < 0.05$) and in non-enhancing lesions only 0.03 ($p < 0.001$). The T_2^* values of axonal and interstitial water both showed a significant increase in lesions compared with NAWM ($\Delta T_{2,2}^* \sim 27\text{ms}$, $p < 0.001$; $\Delta T_{2,3}^* \sim 12\text{ms}$, $p < 0.05$). The Δf values were lower by ~2.3 Hz ($p < 0.001$) for axonal water in both enhancing and non-enhancing lesions when compared to
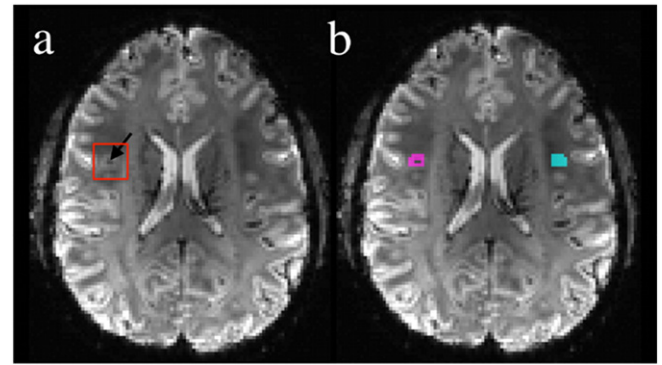

Fig. 2. Example ROI selection for MS lesion and its contralateral NAWM. Lesion (red rectangle) with a visible vein (black arrow) was identified on the normalized T_2^*-weighted mGRE ($S_{TE = 33.6}$) magnitude image (a). Lesion ROI (purple) and ROI in contralateral NAWM with matching geometry (blue) (b).

NAWM. No significant difference between enhancing and non-enhancing lesions was found for any of the parameters studied, including the amplitudes of myelin, axonal, and interstitial water (A_1, A_2, and A_3), the T_2^* values of interstitial and axonal water, or Δf of axonal water.

4. Discussion

In this exploratory study, we investigated the effects of demyelination on T_2^* relaxation in a clinical MS cohort at 7 T. Our 3-compartment model of white matter allowed reproducible fitting of the T_2^* decay curves, demonstrating the feasibility to detect and potentially discriminate demyelination in MS.

The results obtained here for ROIs in SCC are consistent with our previous study in healthy volunteers (Sati et al., 2013), which confirm that T_2^* decay curves can be adequately described by a three-component model with distinct relaxation rates and frequency shifts for each component. Our average value for the amplitude of myelin water (A_1) in SCC was around 0.12, which is also consistent with previous studies using both T_2-based (Whittall et al., 1997; Vavasour et al., 1998; Laule et al., 2004) and T_2^*-based methods (Du et al., 2007; Hwang et al., 2010). In addition, our average value for the myelin water amplitude measured in NAWM ROIs (around 0.10) is also similar to a previous report in healthy volunteers (Hwang et al., 2010).

Our values for the multiple frequencies in SCC are also consistent with our previous results (Sati et al., 2013) and with similar results from another group (Wharton and Bowtell, 2013). As expected, the mean frequency shift is largest for the myelin water compartment (Table 2) due to the perpendicular orientation of the SCC fibers relative the static B_0 magnetic field. Note that this myelin frequency shift is strongly dependent on the fiber orientation (Lee et al., 2010; Sati et al., 2013; Duyn, 2014). Therefore, the NAWM ROIs used here, which in general contain a wider mix of fiber orientations, were expected to display a lower mean value and larger variation for the myelin water frequency shift when compared to the more directionally aligned fibers in SCC and OR (Table 2). As NAWM in MS patients may harbor undetected pathology, the lower frequency shift of myelin water compared to healthy brain might be related to reductions in myelin as well.

In both types of lesion ROIs (enhancing and non-enhancing), our finding of a significant decrease in the amplitude of myelin water suggests ongoing demyelination in these lesions. Note that because the myelin water signal in the lesions was very small, the parameters $T_{2,1}^*$ and Δf_1 were fixed to the reference values obtained from fitting of the contralateral NAWM ROIs. No significant change for fitting results while using different fixed values (supplementary table), which supports that taking the fixed parameters is not a major issue and not a cause for the small numbers of myelin water fraction. Interestingly, the
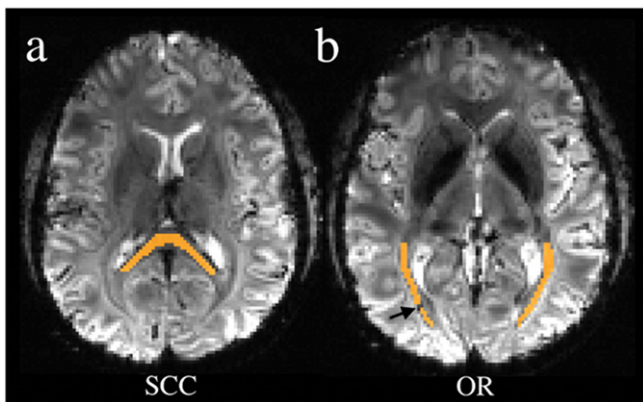

Fig. 1. Example of ROI selection for SCC (a) and OR (b). ROIs (green) were drawn manually on T_2^*-weighted mGRE magnitude images (20th echo with TE = 33.6 ms). The black arrow indicates a visible vein in right OR that was excluded from the ROI.
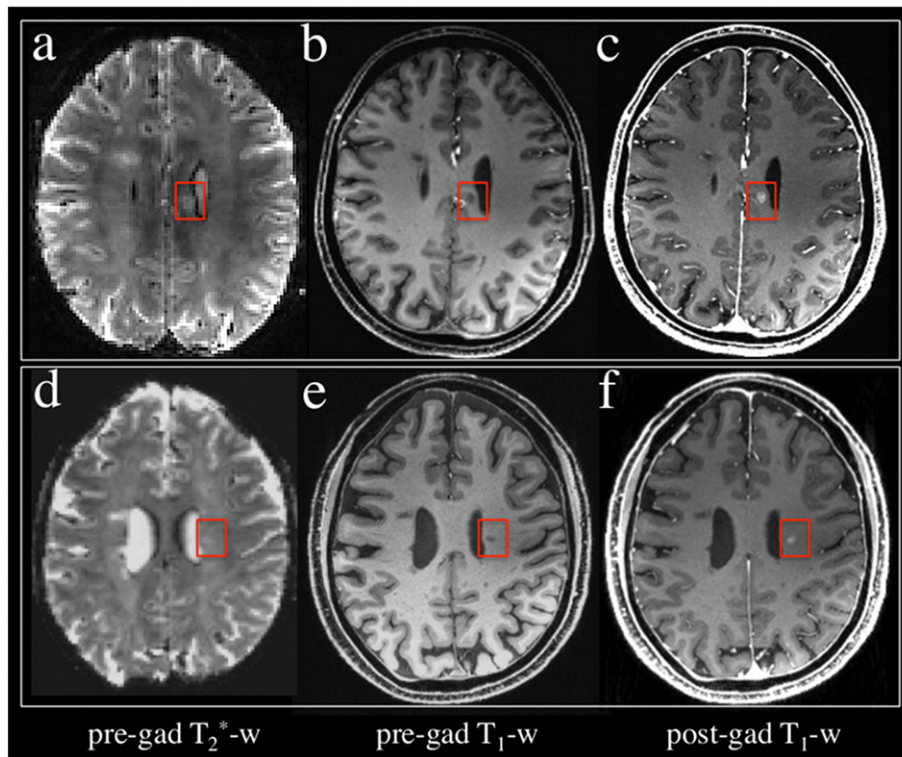
Fig. 3. Identification of two enhancing lesions. The lesions (red rectangle) appear on normalized pre-gad T_2^*-weighted mGRE magnitude ($S_{TE = 33.6}$) (a and d), pre-gad T_1-weighted MPRAGE (b and e), as well as on post-gad T_1-weighted MPRAGE (c and f).

standard deviation (SD) of myelin water amplitude was found to be around 0.02, which is quite large compared to the average myelin water amplitude in lesions but similar to the SD of the fitted myelin water amplitude in SCC and NAWM. This suggests that our estimate of the myelin water amplitudes is reasonable and probably could imply different degrees of demyelination in lesions, while the precision of these amplitude estimates is limited by sensitivity. At the same time, our estimate of the myelin water fraction in lesions is lower than found previously using a T_2-based method (Laule et al., 2004). This discrepancy could result from various factors, including methodological differences: for example, a loss of anisotropic susceptibility in the lesion could reduce the distinction between the water pools.

A positive correlation between total water amplitude and $S_{TE = 33.6}$ was found when combining data from both lesions and NAWM, which indicates that lesions have higher proton density and/or increased T_2^* due to more water than NAWM. However, this correlation was not apparent within the lesion group. It is possible that, in some of the lesions of the current patient cohort, the effects of myelin loss on $S_{TE = 33.6}$ are overwhelmed by the presence of CSF-like interstitial fluid with very long T_2^* as is sometimes seen in chronic lesions.

Our finding of a significant increase in the amplitude of both interstitial and axonal water compartments of the lesions is interpreted as water moving from between myelin layers to the extracellular and/or axonal compartments during the demyelination process. Myelin loss may cause relatively large changes in T_2^* because of the diamagnetic properties of myelin (Stanisz et al., 1999), and because myelin compartmentalizes water and thereby reduces diffusion-mediated averaging of the associated magnetic field inhomogeneities. The frequency shifts of the three signal components are related to the myelin content. The separation of interstitial and axonal water in lesions is expected to be affected by the significantly reduced myelin content, which can lead to a reduced frequency offset between axonal and interstitial water that was expected (Table 2). However, the similar SD of the fitted amplitudes of interstitial and axonal water in lesions when compared to SCC suggests that these components were separated fairly well within lesions.

Increased T_2^* was demonstrated to correspond to severe loss of myelin in comparisons of MRI with histology in MS lesions (Yao et al., 2012; Lee et al., 2012). In our study, the T_2^* of interstitial and axonal water showed a significant increase in lesions compared to NAWM (around 27 and 12 ms respectively), which suggested myelin loss. Moreover, in MS lesions, Δf values were found to be smaller for axonal water relative to NAWM, consistent with myelin loss (Yablonskiy et al., 2012).

We did not find any significant difference between enhancing and non-enhancing lesions for any of the compartmental amplitudes, for T_2^* of interstitial and axonal water, or for Δf of axonal water. If we assume that enhancement reflects an inflammatory process that accompanies ongoing demyelination, and thus that non-enhancing lesions may be more stable and/or partially remyelinated, one would expect this to be reflected in the T_2^* decay characteristics. However, the increased SDs of the component parameters in both enhancing and non-enhancing lesions compared to contralateral NAWM, suggest that the
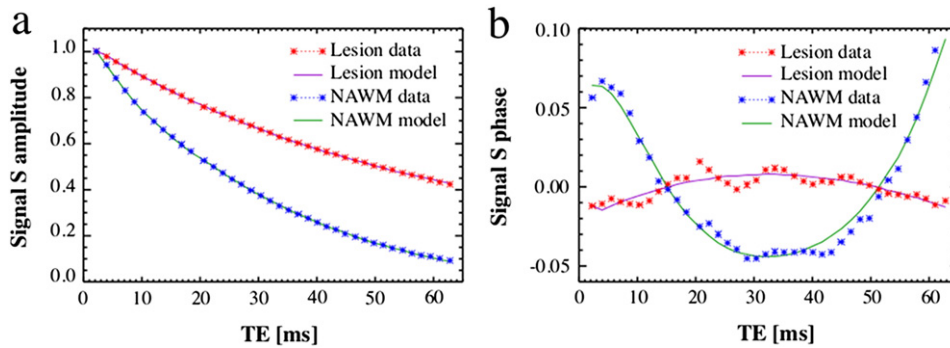
Table 1
Relevant parameters for ROIs used for fitting the three-component model to the T_2^* decay curve. Volume indicates ROI size, SNR the average signal-to-noise ratio of voxels within ROI. Goodness of fit is assessed both using 1-R^2, where R^2 is the coefficient of determination, and the ratio of residue-to-noise, which refers to the difference between temporal standard deviation of the residue of the fitting and the actual noise level in the ROI-averaged signal. The results are shown as mean $\pm$ standard deviation (SD) over N ROIs.

ROI	N	Volume (mm^3)	SNR	1-R^2 (E−04)	Ratio of residue/noise
SCC	25	800.4 ± 265.0	196.2 ± 16.8	0.8 ± 0.4	6.4 ± 1.9
OR	25	655.3 ± 242.0	229.2 ± 20.8	1.4 ± 0.5	9.4 ± 2.8
Enhancing lesion	12	111.4 ± 70.7	244.0 ± 63.0	1.5 ± 1.3	5.2 ± 3.6
Non-enhancing lesion	61	70.2 ± 55.7	224.9 ± 28.5	1.1 ± 1.1	3.0 ± 2.1
Contralateral NAWM	73	73.1 ± 54.7	224.1 ± 32.1	1.3 ± 1.0	2.6 ± 1.3

Fig. 4. Example of a three-compartment model fit to magnitude (a) and phase (b) of ROI-averaged signal S (see the equation) for lesion (red) and contralateral NAWM (blue). Measurement data (symbols) are well matched by the model fit (lines).

absence of significant correlation may be due to a large variation in demyelination within each lesion type, combined with the small number of enhancing lesions included in the analysis.

The fitting of a three-component model to the T_2^* decay curves, as was done here, has several limitations. First, aside from myelin, iron and protein content can also affect T_2^* decay (Duyn et al., 2007), which was not accounted for. Second, the range of TEs in the current study (2.3 ms −62.7 ms) might be suboptimal for fitting long-T_2 components

Table 2

ROI-based fitting of a three-component model to the T_2^* decay curve for SCC, OR, lesion and normal-appearing white matter (NAWM). A_n is the amplitude, $T_{2,n}^*$ the relaxation time (ms), and Δf_n the frequency shift (Hz) of component n. Mean values and the standard deviation (SD) over N ROIs are shown.

ROI	N		Myelin water			Axonal water			Interstitial water	
			A_1	$T_{2,1}^*$ (ms)	Δf_1 (Hz)	A_2	$T_{2,2}^*$ (ms)	Δf_2 (Hz)	A_3	$T_{2,3}^*$ (ms)
SCC	25	Mean	0.12	6.2	25.8	0.47	39.9	−6.3	0.36	30.2
		SD	0.02	0.7	4.6	0.02	3.9	0.6	0.02	4.3
OR	25	Mean	0.10	6.7	22.5	0.49	31.2	−6.5	0.37	46.3
		SD	0.02	0.7	5.2	0.06	1.8	0.7	0.04	9.5
Enhancing lesion	12	Mean	0.03	—	—	0.57	64.0	−3.1	0.40	56.0
		SD	0.02	—	—	0.05	15.1	1.6	0.05	19.1
Non-enhancing lesion	61	Mean	0.04	—	—	0.57	63.0	−3.1	0.37	60.9
		SD	0.02	—	—	0.05	38.4	1.0	0.04	24.9
Contralateral NAWM	73	Mean	0.10	7.6	13.3	0.53	36.0	−5.4	0.34	43.7
		SD	0.02	1.7	9.3	0.04	3.6	0.9	0.04	9.7

present in some lesion types. Third, using results from NAWM as reference values to fix the $T_{2,1}^*$ and Δf_1 of the contralateral lesion may not be accurate, considering that NAWM can have abnormal myelin water amplitude as well (Laule et al., 2004; Oh et al., 2007). This could in principle be mediated by using values from age- and sex-matched healthy volunteers, although accurate delineation of corresponding ROIs would be difficult. Finally, in absence of histopathological evidence, the precise relationship between the amplitude of the short T_2^* component and brain myelin content remains unclear.

5. Conclusions

In summary, fitting of a three-component model to the T_2^* decay curves at high magnetic field allows characterization of myelin water and detection of demyelination in MS. It also provides frequency information of axonal water, which may help to further characterize tissue damage in this disease. The experimental findings reported here are consistent with expectations based on prior radiological and pathological work and further strengthen the cases that analysis of T_2^* decay curves promises to have important consequences for understanding myelin pathology in MS and other neurological disorders.

Supplementary data related to this article can be found online at http://doi.dx.org/10.1016/j.nicl.2015.02.021.

Acknowledgments

Fig. 5. Relationship between fitted myelin water amplitude (A_1) and $S_{TE\,=\,33.6}$. The red and blue points indicate lesions and NAWM respectively.

References

Andrews, T., Lancaster, J.L., Dodd, S.J., Contreras-Sesvold, C., Fox, P.T., 2005. Testing the three-pool white matter model adapted for use with T2 relaxometry. Magn. Reson. Med. 54 (2), 449–454. http://dx.doi.org/10.1002/mrm.2059916032666.

Colin Cameron, A., Windmeijer, F.A.G., 1997. An R-squared measure of goodness of fit for some common nonlinear regression models. Journal of Econometrics 77 (2), 329–342. http://dx.doi.org/10.1016/S0304-4076(96)01818-0.

Du, Y.P., Chu, R., Hwang, D., Brown, M.S., Kleinschmidt-DeMasters, B.K., Singel, D., Simon, J.H., 2007. Fast multislice mapping of the myelin water fraction using multicompartment analysis of T2* decay at 3T: a preliminary postmortem study. Magn. Reson. Med. 58 (5), 865–870. http://dx.doi.org/10.1002/mrm.2140917969125.

Duyn, J.H., 2014. Frequency shifts in the myelin water compartment. Magn. Reson. Med. 71 (6), 1953–1955. http://dx.doi.org/10.1002/mrm.2498324700549.

Duyn, J.H., van Gelderen, P., Li, T.-Q., de Zwart, J.A., Koretsky, A.P., Fukunaga, M., 2007. High-field MRI of brain cortical substructure based on signal phase. Proc. Natl. Acad. Sci. U S A 104 (28), 11796–11801. http://dx.doi.org/10.1073/pnas.061082110417586684.

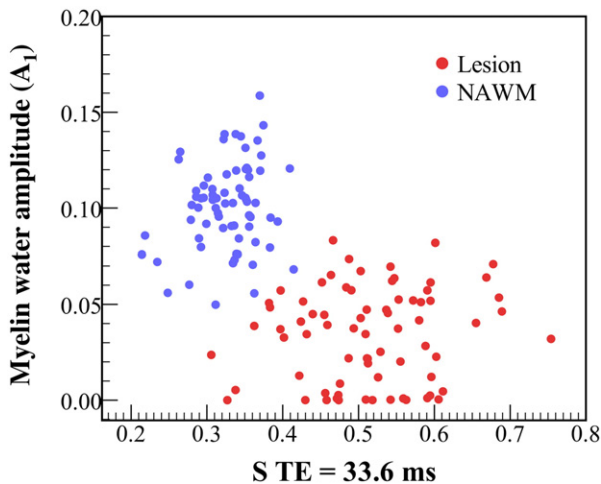Hwang, D., Kim, D.-H., Du, Y.P., 2010. In vivo multi-slice mapping of myelin water content using T2* decay. Neuroimage 52 (1), 198–204. http://dx.doi.org/10.1016/j.neuroimage.2010.04.02320398770.

Lancaster, J.L., Andrews, T., Hardies, L.J., Dodd, S., Fox, P.T., 2003. Three-pool model of white matter. J. Magn. Reson. Imaging 17 (1), 1–10. http://dx.doi.org/10.1002/jmri.1023012500269.

Laule, C., Kozlowski, P., Leung, E., Li, D.K., Mackay, A.L., Moore, G.R., 2008. Myelin water imaging of multiple sclerosis at 7 T: correlations with histopathology. Neuroimage 40 (4), 1575–1580. http://dx.doi.org/10.1016/j.neuroimage.2007.12.00818321730.

Laule, C., Leung, E., Lis, D.K., Traboulsee, A.L., Paty, D.W., MacKay, A.L., Moore, G.R., 2006. Myelin water imaging in multiple sclerosis: quantitative correlations with histopathology. Mult. Scler. 12 (6), 747–753. http://dx.doi.org/10.1177/135245850607092817263002.

Laule, C., Vavasour, I.M., Kolind, S.H., Li, D.K., Traboulsee, T.L., Moore, G.R., MacKay, A.L., 2007. Magnetic resonance imaging of myelin. Neurotherapeutics 4 (3), 460–484. http://dx.doi.org/10.1016/j.nurt.2007.05.00417599712.

Laule, C., Vavasour, I.M., Moore, G.R., Oger, J., Li, D.K., Paty, D.W., MacKay, A.L., 2004. Water content and myelin water fraction in multiple sclerosis. A T2 relaxation study. J. Neurol. 251 (3), 284–293. http://dx.doi.org/10.1007/s00415-004-0306-615015007.

Lee, J., Shmueli, K., Fukunaga, M., van Gelderen, P., Merkle, H., Silva, A.C., Duyn, J.H., 2010. Sensitivity of MRI resonance frequency to the orientation of brain tissue microstructure. Proc. Natl. Acad. Sci. U S A 107 (11), 5130–5135. http://dx.doi.org/10.1073/pnas.091022210720202922.

Lee, J., Shmueli, K., Kang, B.-T., Yao, B., Fukunaga, M., van Gelderen, P., Palumbo, S., Bosetti, F., Silva, A.C., Duyn, J.H., 2012. The contribution of myelin to magnetic susceptibility-weighted contrasts in high-field MRI of the brain. Neuroimage 59 (4), 3967–3975. http://dx.doi.org/10.1016/j.neuroimage.2011.10.07622056461.

MacKay, A., Laule, C., Vavasour, I., Bjarnason, T., Kolind, S., Mädler, B., 2006. Insights into brain microstructure from the T2 distribution. Magn. Reson. Imaging 24 (4), 515–525. http://dx.doi.org/10.1016/j.mri.2005.12.03716677958.

MacKay, A., Whittall, K., Adler, J., Li, D., Paty, D., Graeb, D., 1994. In vivo visualization of myelin water in brain by magnetic resonance. Magn. Reson. Med. 31 (6), 673–677. http://dx.doi.org/10.1002/mrm.19103106148057820.

Moore, G.R., Leung, E., MacKay, A.L., Vavasour, I.M., Whittall, K.P., Cover, K.S., Li, D.K., Hashimoto, S.A., Oger, J., Sprinkle, T.J., Paty, D.W., 2000. A pathology-MRI study of the short-T2 component in formalin-fixed multiple sclerosis brain. Neurology 55 (10), 1506–1510. http://dx.doi.org/10.1212/WNL.55.10.150611094105.

Oh, J., Han, E.T., Lee, M.C., Nelson, S.J., Pelletier, D., 2007. Multislice brain myelin water fractions at 3 T in multiple sclerosis. J Neuroimaging 17 (2), 156–163. http://dx.doi.org/10.1111/j.1552-6569.2007.00098.x17441837.

Pruessmann, K.P., Weiger, M., Scheidegger, M.B., Boesiger, P., 1999. SENSE: sensitivity encoding for fast MRI. Magn. Reson. Med. 42 (5), 952–96210542355.

Sati, P., van Gelderen, P., Silva, A.C., Reich, D.S., Merkle, H., de Zwart, J.A., Duyn, J.H., 2013. Micro-compartment specific T2* relaxation in the brain. Neuroimage 77, 268–278. http://dx.doi.org/10.1016/j.neuroimage.2013.03.00523528924.

Stanisz, G.J., Kecojevic, A., Bronskill, M.J., Henkelman, R.M., 1999. Characterizing white matter with magnetization transfer and T(2). Magn. Reson. Med. 42 (6), 1128–1136. http://dx.doi.org/10.1002/(SICI)1522-2594(199912)42:6<1128::AID-MRM18>3.0.CO;2-910571935.

Van Gelderen, P., de Zwart, J.A., Lee, J., Sati, P., Reich, D.S., Duyn, J.H., 2012. Nonexponential T_2^* decay in white matter. Magn. Reson. Med. 67 (1), 110–117. http://dx.doi.org/10.1002/mrm.2299021630352.

Vavasour, I.M., Whittall, K.P., MacKay, A.L., Li, D.K., Vorobeychik, G., Paty, D.W., 1998. A comparison between magnetization transfer ratios and myelin water percentages in normals and multiple sclerosis patients. Magn. Reson. Med. 40, 763–768.

Wharton, S., Bowtell, R., 2013. Gradient echo based fiber orientation mapping using R2* and frequency difference measurements. Neuroimage 83, 1011–1023. http://dx.doi.org/10.1016/j.neuroimage.2013.07.05423906549.

Whittall, K.P., MacKay, A.L., Graeb, D.A., Nugent, R.A., Li, D.K., Paty, D.W., 1997. In vivo measurement of T2 distributions and water contents in normal human brain. Magn. Reson. Med. 37, 34–43.

Yablonskiy, D.A., Luo, J., Sukstanskii, A.L., Iyer, A., Cross, A.H., 2012. Biophysical mechanisms of MRI signal frequency contrast in multiple sclerosis. Proc. Natl. Acad. Sci. U S A 109 (35), 14212–14217. http://dx.doi.org/10.1073/pnas.120603710922891307.

Yao, B., Bagnato, F., Matsuura, E., Merkle, H., van Gelderen, P., Cantor, F.K., Duyn, J.H., 2012. Chronic multiple sclerosis lesions: characterization with high-field-strength MR imaging. Radiology 262 (1), 206–215. http://dx.doi.org/10.1148/radiol.1111060122084205.